Carbohydrate Research 384 (2014) 102–111

Contents lists available at ScienceDirect

Carbohydrate Research

journal homepage: www.elsevier.com/locate/carres

Exploring the binding of 4-thiothymidine with human serum albumin by spectroscopy, atomic force microscopy, and molecular modeling methods

Juling Zhang [a], Huaimin Gu [a,*], Xiaohui Zhang [b,*]

[a] MOE Key laboratory of Laser Life Science, College of Biophotonics, South China Normal University, Guangzhou 510631, China
[b] College of Environment and Chemical Engineering, Dalian University, Dalian, Liaoning 116622, China

ARTICLE INFO

Article history:
Received 8 October 2013
Received in revised form 21 November 2013
Accepted 27 November 2013
Available online 4 December 2013

Keywords:
Human serum albumin
S^4TdR
SERS
Atomic force microscopy
Molecular modeling

ABSTRACT

The interaction of 4-thiothymidine (S^4TdR) with human serum albumin (HSA) was studied by equilibrium dialysis under normal physiological conditions. In this work, the mechanism of the interaction between S^4TdR and human serum albumin (HSA) was exploited by fluorescence, UV, CD circular, and SERS spectroscopic. Fluorescence and UV spectroscopy suggest that HSA intensities are significantly decreased when adding S^4TdR to HAS, and the quenching mechanism of the fluorescence is static. Also, the ΔG, ΔH, and ΔS values across temperature indicated that hydrophobic interaction was the predominant binding force. The CD circular results show that there is little change in the secondary structure of HSA except the environment of amino acid changes when adding S^4TdR to HSA. The surface-enhanced Raman scattering (SERS) shows that the interaction between S^4TdR and HSA can be achieved through different binding sites which are probably located in the II A and III A hydrophobic pockets of HSA which correspond to Sudlow's I and II binding sites. In addition, the molecular modeling displays that S^4TdR–HSA complex is stabilized by hydrophobic forces, which result from amino acid residues. The atomic force microscopy results revealed that the single HSA molecular dimensions were larger after interaction of 4-thiothymidine. This work would be useful to understand the state of the transportation, distribution, and metabolism of the anticancer drugs in the human body, and it could provide a useful biochemistry parameter for the development of new anti-cancer drugs and research of pharmacology mechanisms.

1. Introduction

Human serum albumin (HSA), the most abundant protein in plasma, has the major properties of transporting various endogenous and exogenous compounds,[1] such as fatty acids, thyroxine, bilirubin, hormones, bile acids, as well as an extraordinarily broad range of medicines.[2–6] In addition, owing to its clinical and pharmaceutical functions, HSA has been used to target diseased and malignant cells as a versatile drug carrier, resulting in higher efficacy of treatment and reduced side effects.[7–9] Thus, studies on physiologically relevant drug–HSA interactions, especially on the binding sites and affinities, are of intense interest to many of the scientists in the field.[10–13] HSA is a globular protein, and it is composed of three homologous alphahelical domains (I–III), each of which is composed of two subdomains A and B. The albumin is stabled by 17 disulfide bridges.[14] On the basis of Sudlow nomenclature, the initial regions of ligand binding sites in HSA are oriented in hydrophobic cavities in subdomains IIA and IIIA, which are alluded to Sudlow I and Sudlow II, respectively, and the sole tryptophan residue in HSA is located in Sudlow I.[15,16]

This paper investigates the association of HSA with 4-thiothymidine (S^4TdR). S^4TdR consists of 2′-deoxyribose attached to the pyrimidine base 4-thiothymidine (Scheme 1). S^4TdR is a thio analogue of the naturally occurring nucleoside thymidine, in which the oxygen atom at the 4-position is replaced by a sulfur atom. It has a strong absorption in the UVA (320–400 nm) region.[17–19] These two nucleosides have markedly different ultraviolet absorbance spectra. In addition, many promising new drugs are proved ineffective because of their unusually high affinity for this abundant protein.[20] Obviously, a better understanding of the mechanisms by which many classes of pharmaceuticals interact with the protein, could suggest new approaches to drug therapy and design. Despite high potential of S^4TdR as anti-cancer agent,[20] the interaction of HSA with S^4TdR has not yet been thoroughly investigated. Such a study, however, should be useful to understand the binding sites of the different levels of the interactions of pharmacology molecular and HSA, and to obtain the anti-tumor mechanism of S^4TdR.

* Corresponding authors. Tel.: +86 13416416788; fax: +86 85216972.
E-mail addresses: guhm@scnu.edu.cn, guhm139@139.com (H. Gu).

0008-6215/$ - see front matter © 2013 Elsevier Ltd. All rights reserved.
http://dx.doi.org/10.1016/j.carres.2013.11.018

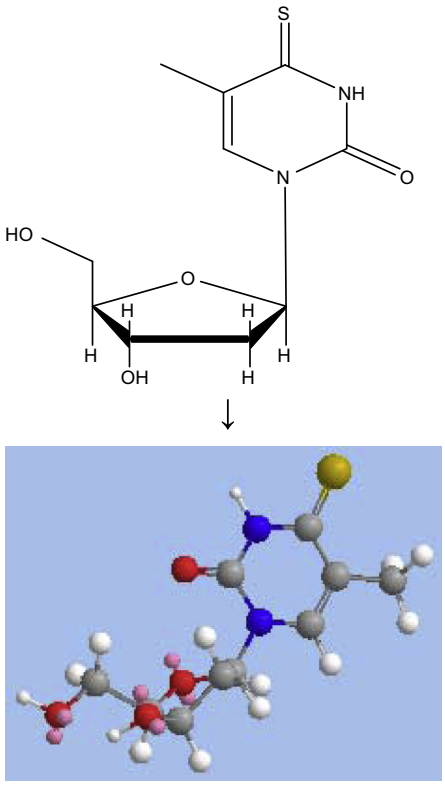

Scheme 1. The structure of the S^4TdR.

In this paper, we report our findings, from the interactions between S^4TdR and albumin using surface-enhanced Raman spectroscopy (SERS), which shows the influence of the pH value of the S^4TdR and the different ratio of the HSA–S^4TdR on the interaction. These results suggest that the change of the structure of the S^4TdR at different pH is similar to that of the interaction between S^4TdR and HSA. The interaction of the thio analogue anti-tumor drug and HSA was studied first in this paper, whereby the mechanism of the interaction between S^4TdR and HSA was systemically analyzed to deduce the probable binding site of S^4TdR on HSA in different concentrations when the interaction takes place spontaneously. Meanwhile, the interactions at different pH values were also studied.

In short, the interaction of S^4TdR with HSA was investigated by using fluorescence spectra, UV, Circular dichroism (CD), SERS, Atomic force microscopy (AFM) and Molecular modeling methods in this study. These spectroscopic techniques and methods provide the important information to study the mechanism of interaction between drugs and biomacromolecules.

2. Results and discussion

2.1. Normal Raman and SERS spectra of S^4TdR–HSA complex

For a better understanding of the SERS spectra of S^4TdR–HSA complex at different concentrations, the NR and SERS spectrum of S^4TdR are indispensable. The NR spectrum of S^4TdR solution and the colloid SERS spectrum are compared in Figure 1 (600–1800 cm^{-1}). The reason for choosing excitation at 632.8 nm for S^4TdR solution is that this molecule is in fact extremely fluorescent at 514 nm excitation, and the resulting background obscures its Raman spectrum. The highly enhanced modes in SERS spectra especially in the region of longer wavenumbers (Fig. 1) are due to the vibration of molecule system and the C=S bending deformation, and it implies that the ring system of S^4TdR is parallel to the

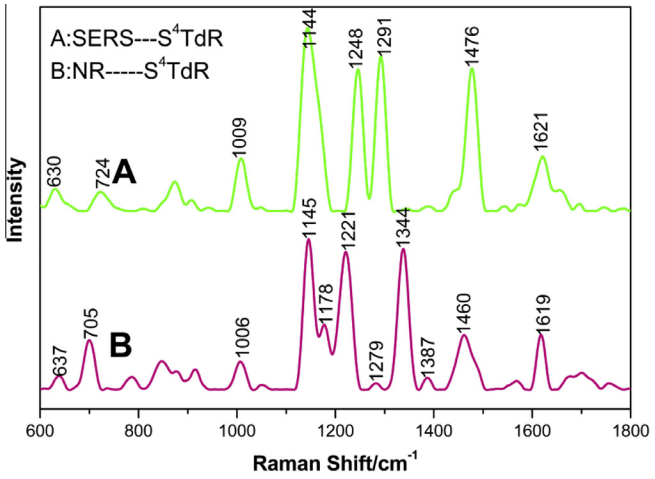

Figure 1. Normal Raman (excitation at 632.8 nm $C = 10^{-3}$ mol/L) and SERS (excitation at 632.8 nm $C = 1.2 \times 10^{-6}$ mol/L) spectra of berberine in the region of 600–1800 cm^{-1}.

surface of Au colloid when S^4TdR is adsorbed on metal surface according to the selection rules.[21] In addition, the line at 1476 cm^{-1} can be assigned as the out-of-plane S^4TdR molecule asymmetric bend and it is also strongly enhanced in SERS, which provides additional evidence of spatial orientation of S^4TdR. According to the surface selection rule in SERS,[21] only vibrations with a component perpendicular to the metal surface can interact with the surface electric field and consequently shows a Raman activity in SERS. Thus, it is reasonable to believe that the S^4TdR plane assumes a parallel or nearly parallel orientation to the Au surface with the S atom and N1 atom tilted slightly with respect to the surface normal. This phenomenon is further supported by the band at 1291 cm^{-1} due to the vibration of C5-Me of S^4TdR molecule, while the peak is too weak to be observed in the NR spectrum. This is probably due to the slight angle between the heterocyclic ring and colloid particle in NR, whereby the heterocyclic ring is approximately paralleled to the metal surface in SERS. Thus, this S^4TdR molecule is oriented flat on the metal surface with the heterocyclic ring inclined. In addition, the band at 1344 cm^{-1} in the NR spectrum may be attributed to out-of-plane sugar molecule scissor and heterocyclic symmetric bend. They are both hardly enhanced in the SERS spectrum. This phenomenon suggests that these two vibrational modes are almost parallel to the surface of the Au colloid. From Figure 1, it is evident that band under 720 cm^{-1} in NR spectra is relatively strong, but rather too weak in SERS. This might suggest that the sugar ring is not completely absorbed on the surface of the Au colloid.

2.2. UV–visible Absorption of S^4TdR and its albumin complexes

The UV–visible absorption spectra of free S^4TdR at different pHs are shown in Figure 2. Three S^4TdR species (acidic, basic, and neutral) can be observed with characteristic maximum at 335 nm, 334 nm, and 315 nm respectively. As the pH values decrease, the intensity and peak of the absorption change. The 315 nm absorbance band of S^4TdR at pH 12.23 shifts to 334 nm at pH 7.09 and to 335 nm at pH 2.23, it may be due to the transition of n–π^* R, the neutral pH would reflect the physiological condition, and thus used for studying the S^4TdR–HSA complex. Figure 3 shows the absorption spectra of S^4TdR (**line A**), HSA (**line C**) and their complex (**line B**) are displayed in Figure 3B. The absorption spectrum of the S^4TdR–HSA complex is similar to that of the S^4TdR at neutral pH with a maximum at 332 nm. It indicates that the drug remains the same in the S^4TdR–HSA complexes.

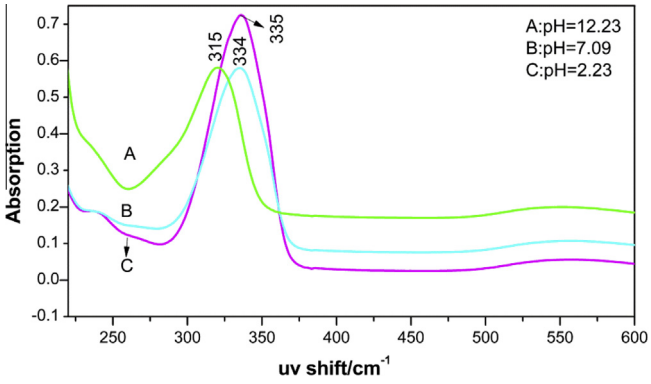

Figure 2. UV–visible absorption spectra of S^{4}TdR at pH 12.23 (A), 7.09 (B), 2.23 (C).

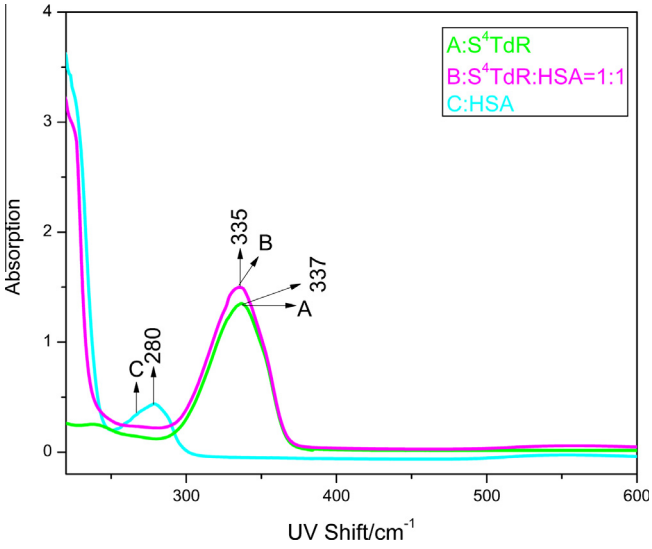

Figure 3. UV–vis spectra of HSA in the presence S^{4}TdR (B), S^{4}TdR (A) only and HSA only (C); C (S^{4}TdR): C (HSA) = 1:1.

2.3. Fluorescence quenching

The intrinsic fluorescence of HSA mainly results from the tryptophan (Trp) residue. The phenylalanine residue has a very low quantum yield and the tyrosine residue fluorescence is nearly quenched when it is ionized or near an amino, carboxyl of the Trp group. The HSA intrinsic fluorescence is very susceptible to its microenvironment. A large number of molecular interactions could lead to fluorescence quenching of the HSA, excited state reactions, molecular rearrangements, energy transfer, ground-state complex formation, and collision quenching are included.[22] The fluorescence emission spectra of HSA at various concentrations of 4-thiothymidine are shown in Figure 4. Obviously, HSA has a strong fluorescence emission band at 350 nm at an excitation wavelength of 282 nm, which is mainly due to its single tryptophan residue, while S^{4}TdR has no intrinsic fluorescence under the present experimental conditions. The fluorescence emission intensity of HSA decreases with the addition of S^{4}TdR. The strong quenching of HSA fluorescence clearly indicates that the interaction between S^{4}TdR and HSA takes place and results from microenvironment changes of the tryptophan residues and the tertiary structure of HSA.[23]

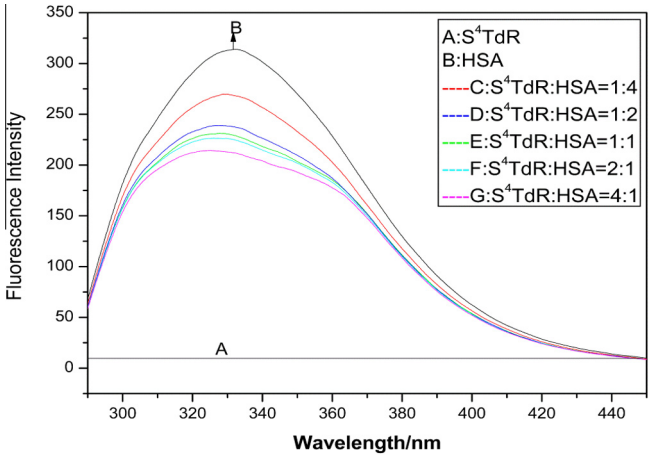

Figure 4. Fluorescence emission spectra of HSA in the presence of different concentrations of S^{4}TdR. C:S^{4}dR-HSA = 1:4 D:S^{4}TdR–HSA = 1:2 E:S^{4}TdR–HSA = 1:1 F:S^{4}TdR–HSA = 2:1 G:S^{4}TdR–HSA = 4:1 A back line and B back line show the emission spectra of HSA and S^{4}TdR only.

2.4. Quenching mechanism

2.4.1. The effect of S^{4}TdR on HSA

A number of molecular interactions can result in quenching, such as ground-state complex formation, excited-state reaction, molecular rearrangements, and collisional quenching. The different mechanisms of quenching can be generally identified as either dynamic or static quenching. Different temperatures and viscosities also influence the dynamic and static quenching.[20] A higher temperature leads to a faster diffusion and hence more dynamic quenching. It can also lead to the dissociation of weakly bound complexes and, thus, less static quenching.

The possible quenching can be studied by the fluorescence quenching spectra of HSA. The $F_0/F - [Q]$ (Stern–Volmer) curves of S^{4}TdR with HSA at different temperatures are shown in Figure 5.

It can be seen from Figure 5 that the Stern–Volmer plots are in liner and the slopes decrease with the increase of temperature. This phenomenon indicates that the interaction between S^{4}TdR and HSA is a static quenching. To confirm this point, the process

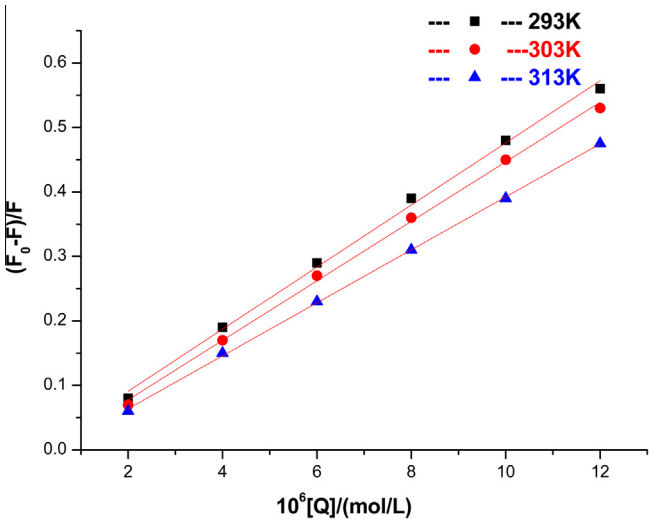

Figure 5. Stern–Volmer plots for the quenching of HSA fluorescence by S^{4}TdR–HSA at three temperatures.

Table 1
Stern–Volmer quenching constants of the interaction between S^4TdR and HSA system at various temperatures

Complex	Temperature (K)	Stern–Volmer equation	K_{sv}	K_q	R	SD
S^4TdR	293	$(F_0 - F)/F = 4.037 \times 10^4[Q] - 0.0629$	4.037×10^4	4.037×10^{12}	0.99949	0.0629
	303	$(F_0 - F)/F = 4.032 \times 10^4[Q] - 0.00237$	4.032×10^4	4.032×10^{12}	0.99823	0.00237
	313	$(F_0 - F)/F = 3.770 \times 10^4[Q] + 0.00241$	3.770×10^4	3.770×10^{12}	0.99917	0.00241

R is the correlation coefficient; SD is the standard deviation.

was assumed to be dynamic quenching. The fluorescence quenching data were analyzed by the Stern–Volmer equation:

$$(F_0/F) = 1 + K_q\ \tau_0\ [Q] = 1 + K_{sv}[Q] \quad (1)$$

where F_0 and F are the fluorescence intensities in the absence and presence of quencher respectively. K_q, K_{sv}, τ_0, and Q are the quenching rate constants of the molecule, the Stern–Volmer quenching constant, the average lifetime of the fluorescence without quencher and with quencher respectively. Obviously,

$$K_{sv} = K_q\tau_0 \quad (2)$$

The result of the lifetimes experiment shows that the life time of the HSA fluorescence is 1.77×10^{-9} s (τ_0 is 1.77×10^{-9} s). The total volume of 4-thiothymidine is less than 50 μL, far less than the volume of HSA (3.0 mL), thus the volume change can be ignored. In addition, an approximately quenching constant (K_q, L mol^{-1} s^{-1}) can be obtained according to Eq. (2). The data results are listed in Table 1 together with correlation coefficients.

The maximum scattered collision quenching constant K_q of various quenchers with HSA is 2.0×10^{10} L mol^{-1} s^{-1}.[24] Evidently, the rate constant of the protein quenching procedure initiated by S^4TdR is greater than that of the scattered procedure. This suggests that the quenching is not initiated by dynamic collision but results from the formation of S^4TdR–HSA complex.

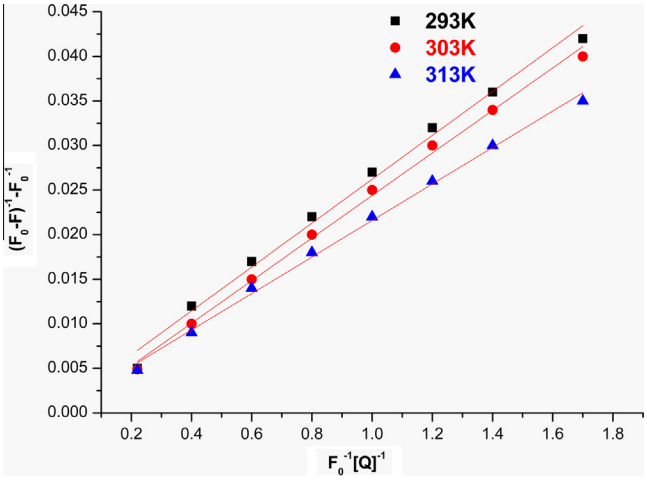

Figure 6. Lineweaver–Burk line for the interaction HSA and S^4TdR.

2.4.2. The binding constants of S^4TdR and HSA

In this work, the binding constants are obtained by using the Lineweaver–Burk equation,[25] which are applied in the discussion of binding modes. The static quenching equation is:

$$(F_0 - F)^{-1} = F_0^{-1} + K_b^{-1}F_0^{-1}[Q]^{-1} \quad (3)$$

where K_b denotes the binding constant of the drug and biomolecule, which can be calculated from the slope and intercept of the Lineweaver–Burk curves as shown in Figure 6 (K_b = intercept/slope). The results are listed in Table 2. These results are in agreement with the above Stern–Volmer equation, and further reveal that the quenching mechanism of S^4TdR–HSA interactions is a static quenching procedure.

2.4.3. Dependence of binding mode between S^4TdR and HSA

The interaction forces between drugs and biomolecules may include multiple hydrogen bonds electrostatic interactions, Van der waals interactions, hydrophobic and steric contacts within the anti-body binding sites.[26] The thermodynamic parameters of the binding reaction provide the main evidence for confirming the interaction forces. Thus, the temperature-dependency of the binding constant was investigated (Fig. 7). The thermodynamic parameters were obtained by using the Van't Hoff equation [Eqs. (4) and (5)]:

$$\ln K = -\Delta H/\mathrm{RT} + \Delta S/R \quad (4)$$

where K is the associative binding constants at the corresponding temperature and R is the gas constant. The temperatures used were 293 K, 303 K and 313 K. Next, the free energy change (ΔG) can be then evaluated from the following equation:

$$\Delta G = \Delta H - T\Delta S = -\mathrm{RT}\ln K \quad (5)$$

The ΔH, ΔS, and ΔG values are listed in Table 3. The ΔH and ΔS values were 11.17 kJ mol^{-1} and 140.32 J mol^{-1} K^{-1} for S^4TdR–HSA, respectively. Timasheff and Subramanian characterized the sign and magnitude of the thermodynamic parameter associated with various protein interactions.[27,28] Considering the water molecule structure theory, a positive ΔS value is frequently regarded as evidence for hydrophobic drug–protein interactions. Thus, the binding for S^4TdR and HSA is mainly based on the hydrophobic interaction.

2.5. The CD spectra of S^4TdR–HSA complex

The secondary structure of the protein molecules caused by some of the reactions was sensitively detected by the circular dichroism spectra. The circular dichroism spectra of S^4TdR–HSA

Table 2
The binding constant K_b of the S^4TdR–HSA system at various temperatures

System	Temperature (K)	Lineweaver–Burk equation	K_b (L/mol)	R
S^4TdR	293	$(F_0 - F)^{-1} - F_0^{-1} = 0.02981F_0^{-1}\ [Q]^{-1} - 0.00230$	3.41×10^7	0.99807
	303	$(F_0 - F)^{-1} - F_0^{-1} = 0.02577F_0^{-1}\ [Q]^{-1} - 1.03673 \times 10^5$	3.92×10^7	0.99386
	313	$(F_0 - F)^{-1} - F_0^{-1} = 0.0242F_0^{-1}\ [Q]^{-1} + 0.00148$	4.33×10^7	0.99987

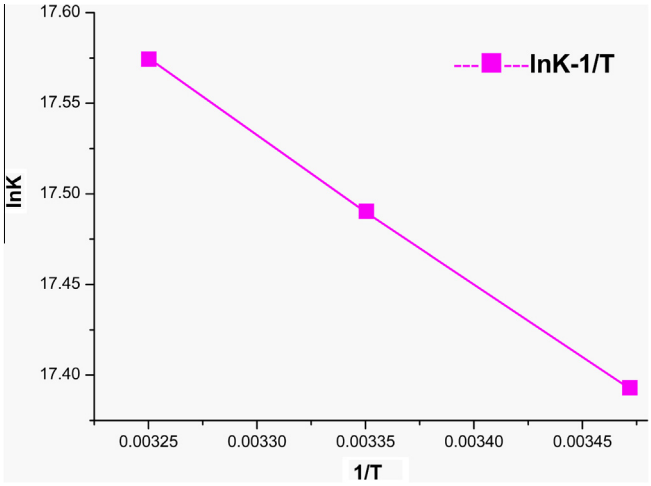

Figure 7. Van't Hoff plot for the interaction of S^4TdR–HSA.

Table 3
The related thermodynamic parameters of the S^4TdR–HSA system at various temperatures

Complex	Temperature (K)	ΔG (kJ/mol)	ΔH (kJ/mol)	ΔS (J mol^{-1} K^{-1})
S^4TdR	293	−29.94	11.17	140.32
	303	−31.35		
	313	−32.75		

complexes are shown in Figure 8. There are two negative bands at 208 nm and 222 nm in the circular dichroism spectra, which is a typical α-helix structure of the CD spectra signal. A reasonable explanation is that the negative peaks at 208 nm and 222 nm both arise from n→π* transfer in the peptide bonds of the α-helix.[29] It can be seen from Figure 8 when the concentration of S^4TdR is gradually increased, the intensity of CD spectra is decreased, in other words, the binding of S^4TdR to HSA decreases the intensities of both of these bands, clearly indicating a decrease in the α-helix content of the protein. In addition, when the S^4TdR is added to the HSA, the secondary structure of the protein molecules HSA

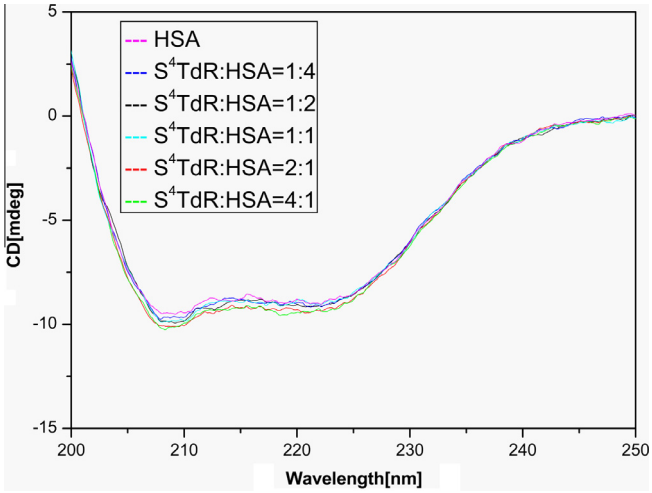

Figure 8. CD circular spectra of HSA in the presence of S^4TdR; magenta line: HSA, blue line:HSA:S^4TdR = 4:1, black line:HSA:S^4TdR = 2:1, cyan line:HSA:S^4TdR = 1:1, red line:HSA:S^4TdR = 1:2, green line:HSA:S^4TdR = 4:1. (For interpretation of the references to color in this figure legend, the reader is referred to the web version of this article.)

Table 4
The conformational changes of HSA determined by S^4TdR spectra

$C_{(S^4TdR)}$ (μmol L^{-1})	α-Helic (%)	β-Sheet (%)	β-Turn (%)	Random coil (%)
0	24.7	34.7	17.8	22.8
0.025	26.7	34.8	14.4	24.0
0.05	24.1	37.0	16.0	23.1
0.1	20.1	39.6	17.9	19.4
0.2	29.5	31.7	15.0	23.9
0.4	31.8	9.6	7.5	35.1

basically has no changes and the circular dichroism spectra also are unchanged basically. We have also calculated the α-helix percentage of HSA and HSA–S^4TdR complex respectively. The α-helix contents of free HSA and its drug complexes were determined and shown in Table 4, indicating a slight change in the secondary structure of protein upon binding to the probe. This indicates that S^4TdR binds with the amino acid residues of the main polypeptide chain of the protein and destroys their hydrogen bonding networks.[30] The results show that S^4TdR in the tumor cells has less effect on the structure of HSA, and there are only little changes in the secondary structure of HAS. These indicate that the kinds of anti-tumor drugs in the human body are almost no change in the secondary structure of HSA. Therefore, HSA is a kind of the carrier protein which can safely carry anti-tumor drugs (S^4TdR) to reach the affected area of tumor cells.[31]

2.6. The UV–vis spectra of S^4TdR–HSA complexes at different concentrations

As known from fluorescence emission spectra of S^4TdR–HSA complexes (Fig. 4), the molecular interaction can result in a quenching of the fluorescence of HSA. However, the mechanism of this phenomenon may be either dynamic quenching or static quenching. To distinguish dynamic and static fluorescence quenching of the S^4TdR–HSA complexes, the UV absorption spectra of HSA and S^4TdR were studied (shown in Fig. 9), and the fluorophore was chosen as a characteristic method. Collisional quenching only affects the excited-states of the flurophore, and so no change in the absorption spectra is expected. Compared with the excited-states, the ground-state of the S^4TdR–HSA complex formation will frequently result in perturbation of the absorption spectra of the fluorophore. In order to examine the probable quenching mechanism of fluorescence of HSA by S^4TdR initiated by ground-state

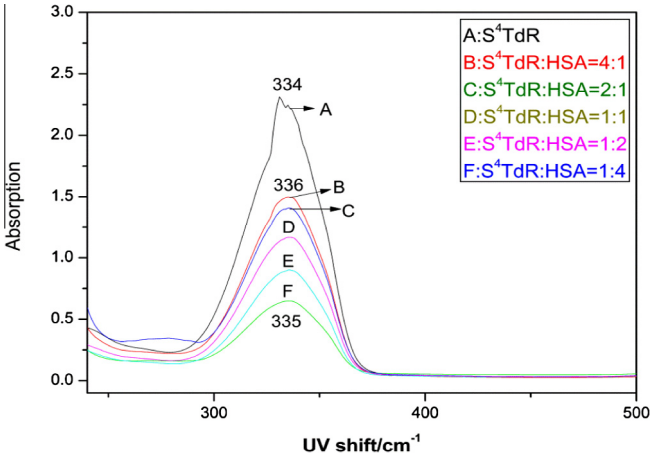

Figure 9. UV–vis spectra of S^4TdR–HSA complex in different ratios of concentration; (B) S^4TdR:HSA = 1:1, (C) S^4TdR:HSA = 1:4, (D) S^4TdR:HSA = 4:1, (E) S^4TdR:HSA = 2:1, (F) S^4TdR:HSA = 1:2.

complex formation, by comparing the UV–vis absorption spectra of HSA and S^{4}TdR–HSA complex at the same concentration, it can be found that they could not be superposed in the range of 280–350 nm, thus, this result offers further support to the proposed static mechanism, by which the fluorescence of HSA is quenched. In addition, the intermolecular interaction corresponding to the fluorescence quenching can also be observed from the absorption spectra.

2.7. SERS of S^{4}TdR at different pH and SERS of S^{4}TdR–HSA complexes at different concentration

SERS Spectra of S^{4}TdR at different pH are shown in Figure 10a(A–C). From Figure 10a, it can be found that the band at 1612 cm^{-1} at pH 2.23 shifts to 1619 cm^{-1} at alkaline pH level. The band 1347 cm^{-1} at pH 2.23 disappears at pH 7.09, and shifts to 1349 cm^{-1} at pH 12.23 which undergo an upward shift. This effect is a consequence of protonation and the electronic resonance increase in the S^{4}TdR.[32] Consequently, the S^{4}TdR species can undergo a nonradiative de-excitation by interaction with the metal or by the formation of an ionic pair. In addition, the band at 1224 cm^{-1} at pH 2.23 shifts to 1247 cm^{-1} at pH 7.09, and moves to 1245 cm^{-1} at pH 12.23. The band at this range is attributed to the Kk stretch. It may be due to the deprotonation of Kk stretch or it is likely that the bond S–N of Kk plane is perpendicular to the Au colloid.

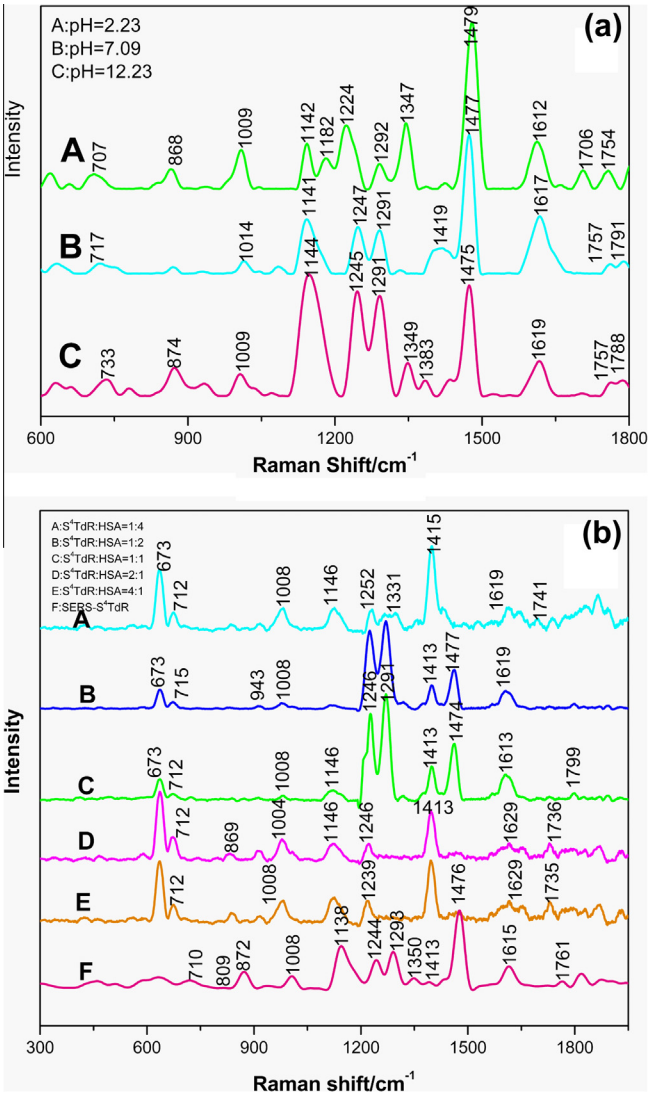

Figure 10. (a) SERS spectra of S^{4}TdR (1 mM) at pH 2.23 (A), 7.09 (B), 12.23 (C); (b) SERS spectra of S^{4}TdR–HSA complex at different concentration ratios in the region of 300–1850 cm^{-1}.

In addition, Figure 10b shows the SERS of S^{4}TdR–HSA complexes at different concentrations. From Figure 10b(A) to Figure 10b(E), the concentration of HSA is constant, while the concentration of S^{4}TdR is gradually increased. Except for the vibrations of DMSO, the SERS spectra of S^{4}TdR are mainly located at 1146, 1246, 1291, and 1477 cm^{-1}. The most characteristic peak embodying the orientation of S^{4}TdR is the line at 1146 cm^{-1}, which accounts for the ring breath and C=S stretch. This band is hardly enhanced in the low concentration (S^{4}TdR–HSA = 1:2), while in the high concentration (1:1, 2:1, 4:1), the intensity increases gradually. This confirms that no matter what the concentration of S^{4}TdR is, the plane of S^{4}TdR molecule is almost perpendicular to the surface of Au nanoparticles. As the spontaneous binding of anti-tumor molecules with HSA takes place initially, then, the S^{4}TdR–HSA complex adsorbs on the surface of Au nanoparticles. In accordance with the result of fluorescence, with the addition of S^{4}TdR solution, the fluorescence intensity decreases gradually. On the basis of the phenomenon, S^{4}TdR has been embodied into the hydrophobic cavity present in HSA. Thus, we can indirectly suggest that when the automatic interaction between S^{4}TdR and HSA takes place, the plane of S^{4}TdR is always perpendicular to the hydrophobic site of HSA. In addition, the bands at 1246, 1291 and 1477 cm^{-1}are weak or even disappear at high concentrations of S^{4}TdR (2:1, 4:1). At the concentration of 1:1, 1:2, the intensity of the heterocyclic ring and C5-Me is slightly enhanced, it can be interpreted that the heterocyclic ring is parallel to the Au nanoparticle at high concentrations, while at lower concentration, the plane of the heterocyclic ring is almost perpendicular to Au nanoparticle, when the automatic binding takes place. This phenomenon may be that the angle between heterocyclic ring and C=S stretch is related to the protein local circumstance and amino acid consequence nearby. In addition, the UV spectra of S^{4}TdR–HSA complexes are displayed in Figure 9. Some bands change evidently at different ratios. From the Figure 10a and b, it can be found that the multiple SERS spectra of Figure 10b show very high similarity to the SERS of S^{4}TdR at different pH.

The SERS spectra of the 1:4 and 1:1 S^{4}TdR–HSA complexes are very similar to the SERS of S^{4}TdR at alkaline pH 12.23. At the ratio of 1:2, 2:1, 4:1 the SERS of S^{4}TdR–HSA complexes is very similar to the SERS of S^{4}TdR at acidic pH 2.23. This phenomenon confirms that the S^{4}TdR molecule has the characteristic binding to HSA which undergo the formation of C–S$^-$ or C–O$^-$ in subdomain II. The spectra of Figure 10a and b indicate that there are two binding sites between S^{4}TdR and HSA, one is the fatty acid in HSA, while the other is defatty acid. With respect to this, it is important to know some aspects of the binding site of protein.

It is generally accepted that the initial binding of small aromatic ligands in HSA settled in subdomains II A and III A,[20] which are consistent with the I and II Sudlow sites.[33] So, S^{4}TdR may interact with HSA at one or two of these sites. On the other hand, HSA's initial binding sites corresponding to fatty acid are placed in subdomain I B, II A and III B,[20] with III A being the most important.[34] Hence, fatty acid and S^{4}TdR have a common binding site in site II. Since the presence of fatty acid in HSA probably changes the structure of S^{4}TdR in the S^{4}TdR–HSA complexes, it may suggest that the initial binding site of S^{4}TdR in defatty HSA corresponds to site II, where S^{4}TdR may interact through electrostatic interaction with the basic aminoacid residues localized in the pocket entrance. Since the S^{4}TdR molecule undergoes the dianionic form in the complex (Fig. 10a(A) and (B), Fig. 10b(C), the intensity of the SERS spectra in Figure 10a(A and B) is weak. This may suggest that

the photoactivity of S^{4}TdR is lower under the monoanionic and dianionic forms.

From Figure 10b(C–E), it can be deduced that site II can be occupied by one or two fatty acid molecules, which may depend on the fatty acid length,[34,20] thus, displacing the S^{4}TdR to site I as also occuring with other ligands displaying the affinity of S^{4}TdR–HSA complexes (1:4, 2:1, 4:1). The spectra of the complexes are similar to that of the acid drug at pH 2.23. It confirms that the S^{4}TdR drug is placed in the hydrophobic cavity of site I, combining with the aminoacid residues therein by means of H-bonds and hydrophobic interactions. In addition, the interaction of the fatty acid with the I B site, which is another initial binding site of the fatty acid, may depend on the interaction of S^{4}TdR with site I since in the I B subdomain site, fatty acid induces a relative rotation of domains I and II of HSA, rendering this site more accessible for the union with antitumor drugs.[35] In conclusion, the intensity of the SERS spectra changes evidently with the addition of S^{4}TdR to the HAS. It can be confirmed that S^{4}TdR molecule has been embodied by HSA. In addition, the SERS spectra of S^{4}TdR–HSA complexes are similar to the SERS of S^{4}TdR at different pH, therefore it can be concluded that the interaction between S^{4}TdR molecule and HAS is completed by means of different anionic forms.

In addition, the SERS of the S^{4}TdR–HAS shown in Figure 10b, Amide III (ca. 1250–1300 cm^{-1}) bands of HSA are also characteristic for the potential α-helical protein. According to the non-resonance conditions, SERS of proteins contain contributions from various amino acid side chain groups. Several of the side chain bands provide information of local side chain conformations or environments. HSA molecule has a single Trp214 at about 1417 cm^{-1}. The band is a marker of the hydrophobicity of the microenvironment of the indole ring. Its intensity changes with increasing hydrophobicity of the environment. SERS spectra suggest that the Trp214 of HSA is a hydrophobic group. To understand visually the binding site between HSA and S^{4}TdR, Figure 11a shows the optimum binding mode and binding site between HSA and S^{4}TdR.

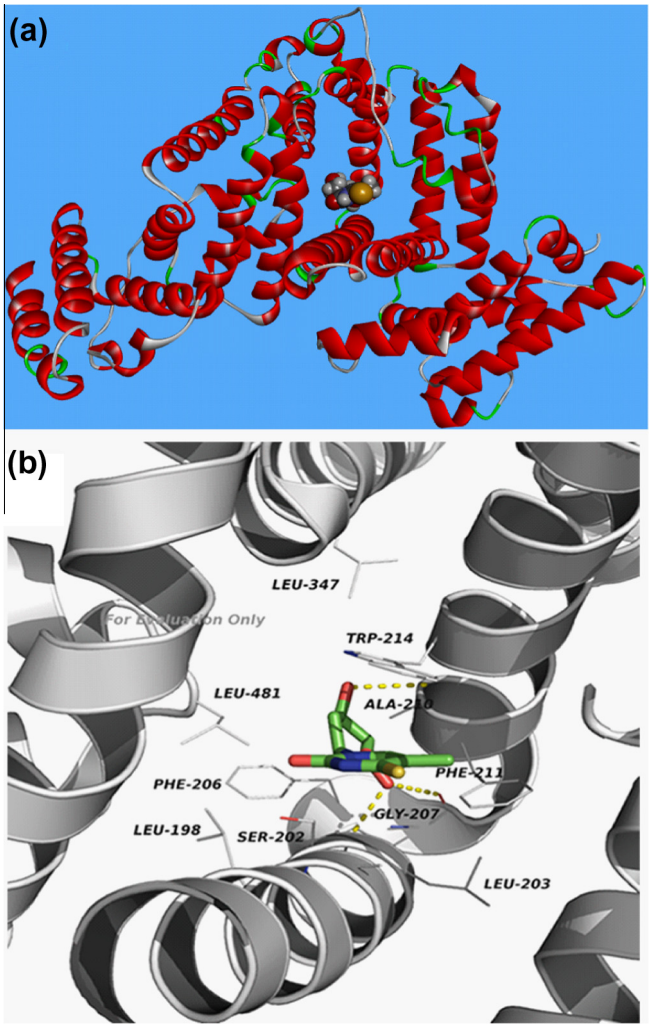

Fig. 11. (a) Molecular docking of S^{4}TdR and HAS; (b) the molecular modeling of interaction between S^{4}TdR and HSA. The residues of HSA are present using gray cartoons. The S^{4}TdR molecule is present using colored sticks. The hydrogen bond between the ligands and the albumin is confirmed by a dashed yellow line. (For interpretation of the references to color in this figure legend, the reader is referred to the web version of this article.)

2.8. Molecular docking study

The crystal structure of HSA is available online. The 3D structure of the crystalline HSA displays the major regions of the ligands binding located in the hydrophobic cavities in the subdomains.[36] Descriptions of the 3D structure of albumin reveal that HSA includes three homologous domains (I–III), I (residues 1–195), II (residues 196–383) and III (residues 384–585), and both the subdomains A and B possess a common structural pattern. It is confirmed that the initial regions of ligands binding to HSA are located in hydrophobic cavities in subdomains IIA and IIIA, which correspond to site I and site II.[37] There is a large hydrophobic cavity present in subdomain IIA that various drugs can bind to. The crystal structure of HSA is from the Brookhaven Protein Data Bank (ID codes: 1H9Z). The structure of HSA is assigned with Kollman-UTI charges in the Amber 4.0 force field. The principle structures of all molecules were generated by molecular docking software SYBYL 6.9.1. The geometries of the compounds were optimized using the Tripos force field with Gsateiger–Marsili charges. AutoDock version 4.2 software was used to compute the interaction between S^{4}TdR and HSA. LGA carried out in AutoDock was applied to compute the possible conformation of the drugs that bind to the albumin. During the actual docking process, a maximum of 10 conformations was considered for this compound. The tautomerism with the lowest binding free energy was used for long-term analysis. Figure 12b shows the results of the best energy ranked. It was evident that the S^{4}TdR molecule lay within subdomain IIA hydrophobic cavity, and the S^{4}TdR is adjacent to hydrophobic residues, for example, Ala (210), Phe (211), Gly (207), Trp (214), etc. The results of molecular docking confirm that the interaction between S^{4}TdR and HSA was controlled by hydrophobic forces, which were in accordance with the binding mode proposed in thermodynamic analysis. In addition, there were several hydrogen bonds between S^{4}TdR and residues of HSA, such as, Gly (207), Ala (210), and Ser (202).

All in all, SERS and CD spectra show that the interaction between S^{4}TdR and HSA does not alter the secondary structure of the protein, but modifies the configuration of at least two disulfide bridges. Interaction with S^{4}TdR moves a single Trp214 of HSA (located within the IIA subdomain) from the more hydrophobic (in HSA) to the hydrophilic surroundings.

2.9. The interaction between S^{4}TdR and HSA based on atomic force microscopy

To understand the changes in HSA topography following the addition of S^{4}TdR, atomic force microscopy was performed on the free HSA and HSA-S^{4}TdR complexes in duplicate. Figure 12 displays the results for the free HSA and its complexes in the Tris–HCl buffer solution.

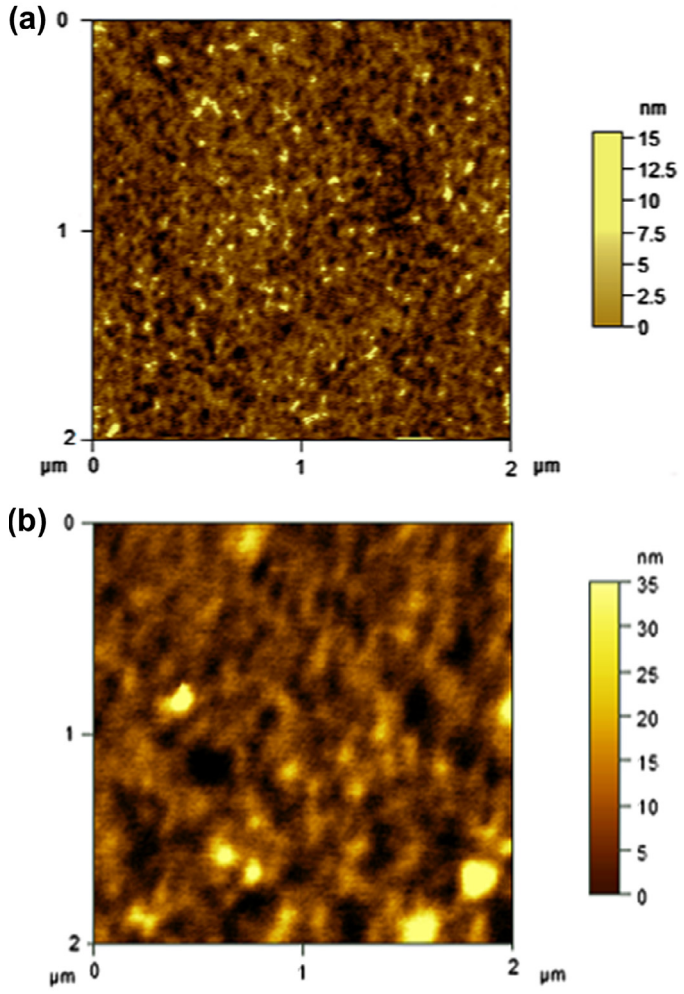

Figure 12. (a) The AFM topography image of free HSA (the light dots); (b) the AFM topography images of the HAS–S^4TdR complex samples were absorbed onto mica during taping mode in a Tris–buffer solution and the scan size of the image is 2 μm × 2 μm.

As shown in Figure 12a, the HSA is absorbed on the mica surface. The mean height of the single HSA molecules is about 5.0 ± 2.8 nm. The dimension is consistent with those from previous AFM reports.[38] Figure 12b shows atomic force microscopy image of the HSA–S^4TdR complex. The majorities of the particles are spherical with hardly any irregularities in shape. The different shapes and size distributions point toward distinctly different forms of morphology of free HSA, S^4TdR, and HSA–S^4TdR complex. The result of AFM image again supports the formation of protein probe complex with morphology totally different from that of the free probe or the free protein. After the addition of S^4TdR, the HSA molecule becomes swollen, the mean height of the HSA reaches about 15.0 ± 4.5 nm (b). The measurement of the HSA–S^4TdR complexation suggests that the molecule of S^4TdR changes the distance between the residues in HSA. Besides, we also observed the aggregation of HSA molecule on the mica substrate for S^4TdR–HSA complexation. Most proteins are aggregated under some special conditions such as appropriate pH value, special composition ion and appropriate concentration of the protein solution. Furthermore, protein–protein hydrophobic interaction is an important factor to cause proteins aggregation.[39] In addition, after interacting of HSA with the S^4TdR, the microenvironment around the HSA becomes more hydrophobic. To minimize the number of unfavorable factors for the formation of a stable structure, the HSA molecule reduces its surface area on contact with water by molecular aggregation. In addition, these results show that a hydrophobic interaction between HSA and S^4TdR may occur.

3. Conclusions

In this paper, the interaction of S^4TdR with HSA was studied by using different spectroscopic, AFM and molecular modeling methods. The quenching mechanism of fluorescence of HSA caused by S^4TdR is a static quenching procedure. When S^4TdR was added, except the environment of amino acid, little change in the secondary structure of HSA was observed. Hence, a low dose of S^4TdR would not be toxic to HSA, when it is transported into the tumor cell. The CD circular results show that there is little change in the secondary structure of HSA except the environment of amino acid changes when adding S^4TdR to HSA. The SERS spectral experiments suggest that S^4TdR interacts with HSA by means of different binding sites and that S^4TdR is adsorbed on the Au nanoparticles by means of different forms. The changes in SERS intensity of S^4TdR indicate that the S^4TdR molecule is adsorbed on the metal surface with dissociated states and the formation of hydrogen bands. The molecular plane is perpendicular to the metal surface, In addition, as shown in Figure 10a and b, the concentration of S^4TdR–HSA complexes (1:1, 1:2, 1:4) is similar to the SERS spectrum of S^4TdR pH 12.23. The initial interaction site of S^4TdR seems to be site II in defatted acid, where the drug interacts with the basic amino acid residues existing at the entrance of the cavity through its dianionic form. In contrast, the concentration of S^4TdR–HSA complexes (2:1, 4:1) is similar to the SERS spectrum of pH 2.23. The primary interaction site of S^4TdR seems to be site I in fatty acid, where S^4TdR interacts with the protein through its acid form in the hydrophobic cavity of this site. S^4TdR may interact with HSA through the H-bond, affecting both the interaction between NH–, C=O groups, and amino acid residues existing in this cavity. Since under physiological conditions the albumin molecules can transport fatty acid, it can be concluded that S^4TdR may be transported by serum albumin in subdomain I. In addition, the molecular modeling displays that S^4TdR–HSA complex is stabilized by hydrophobic forces, which results from amino acid residues. The atomic force microscopy results revealed that the single HSA molecule dimensions were larger after interaction of 4-thiothymidine.

In short, the different spectroscopic, AFM and molecular modeling studies have revealed important data concerning the interaction of anti-tumor drugs of the analogue with albumin of different origins. Further, this paper has special importance in pharmacology and clinical medicine as well as methodology.

4. Experimental

4.1. Materials

4-Thiothymidine was synthesized in Scheme 2 below. The chemicals were used without further purification. Tri-distilled water was used for all solution preparations. HSA was purchased from Sigma–Aldrich, The pH values were checked with a suitably standardized pH meter. All reagents were of analytical degree and triple distilled water was always employed for the solutions.

4.2. Samples for surface-enhanced Raman spectroscopy measurements

100 mL of 1 mM $HAuCl_4$ aqueous solution was stirred and heated to boiling. Next, 6 mL of freshly prepared 38.8 mM tri-sodium citrate solution was added. The mixture was then kept boiling for 20 min. Finally, the solution was cooled down to room

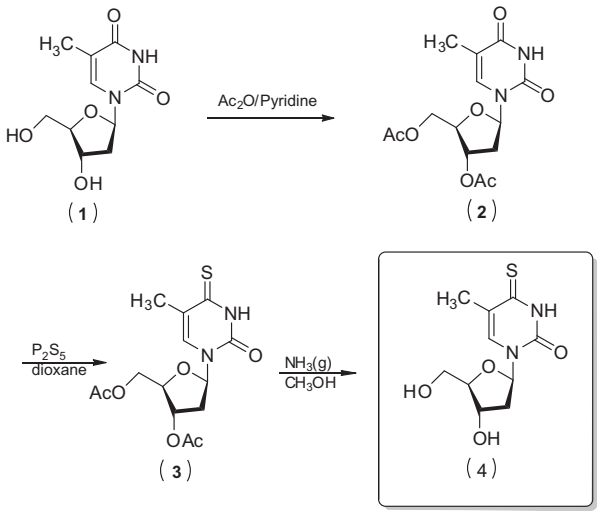

Scheme 2. The route of S^4TdR (4-thiothymidine).

temperature with continuous stirring. The resulting red gold nanoparticles were obtained with the diameter at ca. 30 nm. Samples for macro-SERS experiments were prepared by solving 6 mg of HSA in 1 mL of water. Then, an aliquot of a 10^{-3} M S^4TdR solution in dimethylsulfoxide (DMSO) was added to obtain 1:2, 1:1, 1:4, 2:1, 4:1 S^4TdR–HSA complexes. For these relative concentration complexes, a complete interaction of the anti-tumor drug and the protein is ensured within approximately 12 h. Samples containing only drug were also aged for the same time under the same conditions. The gold colloid was activated before being added to the S^4TdR–HSA complexes. The colloid was also activated before being added to the drug–HSA complex solution by adding 30 μL of 0.5 M nitrate solution to 1 mL of the original colloid. Afterward, 270 μL of this activated colloid was added to the S^4TdR–HSA complexes leading to further dissolution of the above complex to a final ratio of 1.8×10^{-5}:3.6×10^{-5} and 1.2×10^{-5}:4.8×10^{-5} M for the S^4TdR–HSA complexes. These samples were left for one and a half hours at room temperature before starting the measurements to allow the complete diffusion of the complex to the surface. SERS of S^4TdR at different pH were obtained by adjusting the final pH with HCl or NaOH.

4.3. Instrumentation

4.3.1. Surface enhanced Raman spectra (SERS)

SERS spectra were recorded by using LabRAM Aramisa (HJY Co., France) micro-Raman spectrophotometer. The spectral resolution was set to 4 cm^{-1}, and a 180° geometry was used to collect the spectra signal. The excitation laser was 632.8 nm He–Ne laser, and the laser power at the sample was fixed at 2 mW. The spectra signal was calibrated by using the 520 cm^{-1} line of a Si wafer. All the samples for SERS measurements were placed in concavity slides. And the exposure time was set to 10 s and the acquisition times were 3. Spectra were recorded in the 600–1800 cm^{-1} region.

4.3.2. UV–vis absorption spectra

UV–vis absorption measurement was employed to estimate the shape and quality of the Au colloid that served as the enhancing substrate. The UV–vis spectra of the colloids were obtained by employing a UV–vis spectrophotometer (Lambda 35 UV–vis spectrophotometer, Perkin–Elmer, USA) with a scan speed of 240 nm min^{-1}. And the samples were placed in a 1-cm-pathlength quartz ce.

4.3.3. Fluorescence spectra

The fluorescence spectra were measured by RF-5301PC spectrofluorophotometer (Shimadzu, Japan) equipped with 1.0 cm quartz cells. The widths of the excitation slit and the emission slit were set to 5 nm and 3 nm, respectively. Circular dichroism (CD) measurements were performed on a JASCO-J-810 Spectropolarimeter.

4.3.4. CD spectra

Circular dichroism (CD) measurements were performed with a J-810 Spectropolarimeter (Jasco, Tokyo, Japan) at 297 K. CD measurements of HSA in the absence and presence of caffeine were recorded in the range of 260–200 nm. The instrument was controlled by Jasco's Spectra Manager TM software. Quartz cells having path lengths of 0.1 cm were used at a scanning speed of 1000 nm/min. The data were expressed in terms of molar ellipticity[θ]. An appropriate buffer solution run under the same conditions was taken as a blank and subtracted from the sample spectra. Each sample was scanned three times at a bandwidth of 1.0 mm.

4.3.5. Atomicforce microscopy

AFM measurements were carried out with a MutiMode Nanoscope III a (USA) that was equipped with a normal NP probe. The spring constant of the cantilever was 0.32 N/m, and the typical imaging resonance frequency of the fluid was 7–9 KHz. All of the samples were imaged by AFM in fluid contact Mode with an O-ring liquid cell. Samples were prepared as follows: (1) free HSA with 100 μL of 2 μM HAS was added to the mica substrate and incubated for 20 min at 297 K before washing with water and (2) S^4TdR–HSA complexes with free HSA samples were prepared as described in step: prior to adding 100 μL of a 20 μM S^4TdR solution, they were incubated for 20 min and washed with water, and then were dried under N_2 for 5 min and imaged in air with AFM.

4.4. Model docking

According to the Lamarckian Genetic Algorithm,[40] molecular docking simulations were employed with the software package AutoDock version 4.2. Lamarckian Genetic Algorithm was used to calculate the possible conformation of the antitumor drug that binds to the protein in AutoDock. The potential of 3D structure of the HAS complex with warfarin (PDB code 1H9Z) was taken from the Protein Data Bank. The structure of HSA was assigned with Kollman-UTI charges in the Amber 4.0 force field. The initial structures of all the molecules were generated by molecular modeling software Sybyl 6.9.1.[41] The geometries of the antitumor drug were subsequently optimized using the Tripos force field with Gasteiget–Marsili charges. Both initial ligands and molecules were in arbitrary conformation orientation and position. A maximum of 10 conformations was considered for the antitumor drug during the actual docking process. The conformation with the lowest binding free energy was used for further analysis. All calculations were staged on the SCI FUEL workstation.

Acknowledgments

This research was supported by Grants 60678050 from the Nature Science Foundation of China. The work is also financially supported by the Scientific Research Foundation for the Returned Overseas Chinese Scholars, State Education Ministry, PR China.

References

1. Peters, T. *All about Albumin: Biochemistry, Genetics and Medical Application*; Academic Press: San Diego, 1995. p 432.
2. Nicoletti, F. P.; Howes, B. D.; Fittipaldi, M.; Fanali, G.; Fasano, M.; Ascenzi, P.; Smulevich, G. *J. Am. Chem. Soc.* **2008**, *130*, 11677–11688.
3. Abou-Zied, O. K.; Al-Shihi, O. I. K. *J. Am. Chem. Soc.* **2008**, *130*, 10793–10801.

4. Komatsu, T.; Wang, R. M.; Zunszain, P. A.; Curry, S.; Tsuchida, E. *J. Am. Chem. Soc.* **2006**, *128*, 16297–16301.
5. Simard, J. R.; Zunszain, P. A.; Ha, C. E.; Yang, J. S.; Bhagavan, N. V.; Petitpas, I.; Curry, S.; Hamilton, J. *Proc. Natl. Acad. Sci. U.S.A.* **2005**, *102*, 17958–17963.
6. Kragh, H. *Pharmacol. Rev.* **1981**, *33*, 17–53.
7. Elsadek, B.; Kratz, F. *J. Controlled Release* **2012**, *157*, 4–28.
8. Kratz, F.; Elsadek, B. *J. Controlled Release* **2012**, *161*, 429–445.
9. Kratz, F. *J. Controlled Release* **2008**, *132*, 171–183.
10. Chatterjee, T.; Pal, A.; Dey, S.; Chatterjee, B. K.; Chakrabarti, P. *PLoS One* **2012**, *7*, e37468.
11. Hummer, A. A.; Bartel, C.; Arion, V. B.; Jakupec, M. A.; Meyer, K. W.; Geraki, T.; Quinn, P. D.; Mijovilovich, A.; Keppler, B. K.; Rompel, A. *J. Med. Chem.* **2012**, *55*, 5601–5613.
12. Oltersdorf, T.; Elmore, S. W.; Shoemaker, A. R.; Armstrong, R. C.; Augeri, D. J.; Rosenberg, S. H. *Nature* **2005**, *435*, 677–681.
13. Mao, H.; Fesik, S. W. *J. Am. Chem. Soc.* **2001**, *123*, 10429–10435.
14. He, X. M.; Carter, D. C. *Nature* **1992**, *358*, 209.
15. Sudlow, G.; Birkett, D. J.; Wade, D. N. *Mol. Pharmacol.* **1975**, 11–824.
16. Sudlow, G.; Birkett, D. J.; Wade, D. N. *Mol. Pharmacol.* **1976**, 12–1052.
17. Massey, A.; Xu, Y.-Z.; Karran, P. *Curr. Biol.* **2001**, *11*, 1142–1146.
18. Xu, Y.-Z.; Zhang, X.; Wu, H.-C.; Massey, A.; Karran, P. *Bioorg. Med. Chem. Lett.* **2004**, *14*, 995–997.
19. Pridgeon, S. W.; Heer, R.; Taylor, G. A.; Newell, D. R.; Toole, K. O.; Robinson, M.; Xu, Y.-Z.; Karran, P.; Boddy, A. V. *Br. J. Cancer* **2011**, *104*, 1869–1876.
20. Carter, D. C.; Ho, J. X. *Adv. Protein Chem.* **1994**, *45*, 153–203.
21. Lakowicz, J. R. *Principles of Fluorescence Spectroscopy*; Springer: New York, 2006.
22. Tian, J.; Zhao, Y.; Liu, X.; Zhao, S. *Luminescence* **2009**, *24*, 386–393.
23. Trynda-Lemiesz, L.; Keppler, B. K.; Koztowski, H. *J. Inorg. Biochem.* **1999**, *73*, 123–128.
24. Ware, W. R. *J. Phys. Chem.* **1962**, *66*, 455–458.
25. Xie, B.; Wan, B. J.; Qin, Z. H. *Chin. J. Spectrosc. Lab.* **2011**, *28*, 764–769.
26. He, X. M.; Carter, D. C. *Nature* **1992**, *358*, 209–215.
27. Timasheff, S. N. Thermodynamic of Protein Interactions. In *Proteins of Biological Fluids*, Peeters, H., Ed.; Pergamon Press: Oxford, 1972.
28. Ross, P. D.; Subramanian, S. *Biochemistry* **1981**, *20*, 3096–3102.
29. Kamat, B. P.; Seetharamappa, J. *J. Pharm. Biomed. Anal.* **2004**, *35*, 655–664.
30. Cui, F. L.; An, J. F.; Li, J. P.; Hu, Z. D. *Bioorg. Med. Chem.* **2004**, *12*, 151–157.
31. Min-yan, P.; Xue-fang, Z.; Hong-yu, C. *Chin. J. Anal. Chem.* **2010**, *7*, 948–952.
32. Xu, Y.-Z.; Swann, P. F. *Anal. Biochem.* **1992**, *204*, 185–189.
33. Sudlow, G.; Dirkett, D. J.; Wade, D. N. *Mol. Pharmacol.* **1976**, *12*, 1052–1061.
34. Bhattacharya, A. A.; Grüne, T.; Curry, S. *J. Mol. Biol.* **2000**, *303*, 721–732.
35. Curry, S.; Brick, P.; Franks, N. P. *Biochim. Biophys. Acta* **1999**, *130*, 131–140.
36. Abou-Zied, O. K.; Al-Shihi, O. I. K. *J. Am. Chem. Soc.* **2008**, *130*, 10793.
37. Carter, D. C.; He, X. M.; Munson, S. H.; Twigg, P. D.; Gernert, K. M.; Broom, M. B.; Miller, T. Y. *Science* **1989**, *244*, 1195–1198.
38. Kowalczyk, D.; Marsault, J. P.; Slomkowski, S. *Colloid Polym. Sci.* **1996**, *274*, 513–519.
39. Privalow, P. L.; Gill, S. J. *Adv. Protein Chem.* **1988**, *39*, 191.
40. Wang, Z. G.; Ling, B. P.; Zhang, R.; Liu, Y. J. *J. Phys. Chem. B* **2008**, *112*, 10033.
41. Louis, S. T. SYBYL *Software Version 6.9.1*; Tripos Associates, 2003.